Accurate Estimation of the Phase Noise of Delay-Based Optoelectronic Oscillators at Close-in Frequency Offsets

Sajad Jahanbakht*

Sajad Jahanbakht is with the Department of Electrical and Computer Engineering, University of Kashan, Address: Kilometer 6 of Ravand Blvd., city of Kashan, Isfahan province, Iran, email: jahanbakht@kashanu.ac.ir, phone: 00983155913441, mobile: 00989127976538

***Abstract*— Delay-based optoelectronic oscillators (OEOs) use the large propagation delays of long optical fibers to produce ultra-low phase noise (PN) radio frequency (RF) oscillations. Most of the OEO-PN analysis approaches in the literature predict a singular value for the output variable's PN-induced power spectral density (PSD) at zero offset frequency from the carrier. The current paper aims to resolve this issue. First the perturbation theory of classical oscillators is generalized to extract the stochastic delay differential equation (SDDE) governing the PN of OEOs. Then the well-known small delay approximation approach is used to derive a stochastic ordinary differential equation (SODE) governing the PN. Using the previously published solutions to this SODE, the PN-PSD of the OEO is extracted in presence of both white and colored noise sources. As the small delay approximation is only valid for small frequency offsets, the obtained PSDs are only accurate at these offsets. This approach avoids the non-physically large values encountered in classical approaches. For larger frequency offsets one can use the classical noise analysis techniques in the literature. The validity of this approach is verified by comparing its results with those in the literature and direct Monte-Carlo simulations.**

***Index Terms*— near carrier, optoelectronic oscillator, phase noise, stochastic calculus, white and colored noise**

1. Introduction

Optoelectronic oscillators (OEOs) are hybrid photonic-electronic systems that are considered promising candidates for producing ultra-low phase noise (PN) radio frequency (RF) oscillations in the microwave or millimeter-wave range [1]. Many OEO structures use long optical fiber delay lines, which are called delay-based OEOs [1-7]. A delay-based OEO may be implemented as a single-loop OEO (SLOEO) [1-3], multi-loop OEO [4, 6], in conjunction with the intentionally induced stimulated Brillouin scattering (SBS) phenomenon [8, 9], or as the newly proposed parity-time symmetric OEO by again using delay-based configurations [10, 11]. Therefor most of the OEO systems are totally or partially based on the delay-based dynamics.

Because the PN is probably the most important figure of merit in OEOs, this paper concentrates on its analysis. Here for simplicity, the case of delay-based SLOEOs is considered. Many methods have been proposed to address the PN analysis of OEOs, such as the methods based on the PN transfer model and control theory [4, 5], the analytical formulations extracted from solving the Langevin equation governing the PN [3, 12, 13], the conversion matrix approach (CMA) [14-16], and the envelope-domain semi Monte Carlo methods [2, 6]. The techniques in [3, 4, 13-16] predict singular values for the power spectral density (PSD) of the PN-induced output noise at the zero offset frequency. Both envelope domain methods in [2, 6] compute only the PSD of the PN itself, not the PSD of the output variable. Therefore, they may predict singular values at very close-in offsets (after a very long required simulation time). These methods requires runtimes in the order of 10 minutes for calculating PN at offset frequencies larger than 1kHz [2, 6]. For smaller offsets, larger runtimes are required. To the best of the author's knowledge, the references [1] and [17] are the only ones that predict a non-singular PSD at zero offset frequency. However, they have shortcomings as mentioned in section III.

The problem of the singular PN at close-in offsets has already been resolved for non-delay-based electronic oscillators using the Floquet theory in conjunction with the rigorous tools of stochastic calculus [18, 19]. These methods have also been adopted for microwave oscillators with distributed elements [20-22]. Here we want to resolve the same issue in the delay-based OEOs. Removing this singularity completes our knowledge about the PN distribution in OEOs.

The equation governing the PN process in OEOs is a stochastic delay differential equation (SDDE), while that of the conventional oscillators is a stochastic ordinary differential equation (SODE). SDDEs are inherently equivalent to infinite-dimensional SODEs; therefore, treating them requires special techniques [23, 24].

The current paper aims to present a rigorous treatment of the PN in delay-based OEOs so that accurate PN PSDs at very close-in frequency offsets are computed. For this purpose, first, the SDDE governing the PN is extracted by a harmonic balance-based perturbation theory (HBPT) of PN used in [20-22] which is here generalized to the case of delay-based oscillation dynamics of the OEOs. To the best of the author's knowledge, this is the first systematic extraction of this SDDE by using HBPT which paves the way to extracting the same equation in other OEO structures such as the multi-loop ones. Then the small-delay approximation approach (SDAA) to the SDDEs [23, 24] is used to derive an equivalent SODE. This SODE is similar to those in

[18, 19], therefore the rigorous results of these references are used to extract the PN-induced PSD at the close-in frequency offsets while avoiding the singularity problem. Both white and colored noise sources can be taken into account. It is shown in the result section that this method can predict accurate results at the close-in offset frequencies but not generally at larger offsets. This is consistent with the fact that the small-delay approximation is only valid at such offsets. For larger frequency offsets such as those of the spurious peaks responses, one can use the classical fast methods of e.g. [3, 4, 5, 13-16]. The validity of the new approach is verified by comparing its results with the Monte Carlo simulation (MCS), the analytical formulation of [3], and the simulation results of [2].

This paper is organized as follows: the extraction of the SDDE governing the PN is addressed in section 2. The PN-analysis approach based on the small-delay approximation is presented in sections 3. Finally, the simulation results and discussions are presented in section 4.

2. EXTRACTING THE SDDE GOVERNING THE PN

This section presents the schematic of the SLOEO, and the method of extracting the equation governing the PN using HBPT of oscillators.

2.1. The dynamics of the SLOEO

The schematic of the delay-based SLOEO is shown in Fig. 1.

Fig.1

The electro-optic modulator (EOM) modulates the intensity of the laser beam by its input RF signal coming from the RF coupler. Then the modulated optical signal passes through a long optical fiber delay line. The considerable delay imposed by the optical fiber delay line results in the extreme sensitivity of the phase of the loop gain on the oscillation frequency, which acts as a resonator with a very high quality factor for producing ultra-low noise oscillations. Also, this sensitivity becomes larger for larger oscillation frequencies resulting in a PN performance nearly independent of the oscillation frequency [1-3]. The photo-detector (PD) extracts the RF modulation of the output signal of the fiber. This RF signal is amplified by the RF amplifier (RFA) to compensate for the losses of the loop, and filtered by the RF band pass filter (RF-BPF) to remove the unwanted harmonics and attenuate the so-called cavity modes except the desired one. The filtered RF signal is fed back to the RF port of the EOM to close the oscillation loop. The phase shifter may be used to finely adjust the oscillation frequency around the filter's center frequency in a free spectral range (FSR) interval, where the FSR is equal to the inverse of the loop delay (mainly the fiber delay). The RF coupler provides a sample of the RF signal. From now on, the RF signal at the EOM input is regarded as the output variable. It is supposed that the RF-BPF significantly attenuates the non-fundamental harmonics of the RF signal such that the output signal is practically single-harmonic [1-6, 14-16].

The noise-less dynamical system of the SLOEO is given by [1, 2, 14-16]:

$$v(t) = f(t) * \left\{ g\left(v(t - t_0)\right) \right\} \qquad (1)$$

where $v(t)$ is the output RF signal, t_0 is the total delay of the loop (mainly the group delay of the fiber), $*$ denotes the convolution, $f(t)$ is the impulse response of the RF-BPF, and $g(.): R \to R$ is a memory-less nonlinear function addressing the nonlinearities of the EOM and photo-detection defined by:

$$g(v) = -k_g \sin\left[\pi \frac{v}{v_\pi} + \phi_0 \right] \qquad (2)$$

where k_g is a gain factor incorporating the gains of the PD and the RFA and the possible losses of the loop, v_π is the RF half-wave voltage of the EOM, and ϕ_0 is the offset phase of it. It is assumed that the OEO has a stable steady-state periodic solution written as $v(t) = A\cos(\omega_0 t)$, where ω_0 is the RF oscillation frequency, and A is its amplitude. Because only the first harmonics at both sides of (1) are present, it can be written as:

$$z(t) * v(t) = g\left(v(t - t_0)\right) \qquad (3)$$

where $z(t)$ denotes the inverse impulse response of the filter, i.e., its frequency response is given by

$$Z(\omega)=\begin{cases}1/F(\omega) & -\omega_0/2\le\omega\le\omega_0/2\\ 0 & \text{otherwise}\end{cases} \quad (4)$$

where $Z(\omega)$ and $F(\omega)$ are the Fourier transforms of $z(t)$ and $f(t)$ respectively. Note that equation (3) is only relevant for frequencies about the fundamental harmonic with a maximum theoretical bandwidth equal to $\omega_0/2$, as presented in equation (4). Therefore, the other possible frequency components generated on the right-hand side (RHS) of equation (3) are discarded in the analysis.

2.2. The perturbation theory in the presence of noise

In the presence of the noise sources, the circuit variables of a free-running oscillator experience perturbations as [18, 19]:

$$v_p(t)=v\left(t+\alpha(t)\right)+\Delta v(t) \quad (5)$$

where $v_p(t)$ denotes the perturbed variable, the large signal term $\alpha(t)$ is the common time delay process responsible for producing the major part of the PN, and $\Delta v(t)$ is a small-signal additive term called the orbital deviation. The term $\Delta v(t)$ characterizes the amplitude noise [18, 19]. However, it also has small effects on the PN, especially at large frequency offsets from the carrier [21].

For simplicity in presenting the main results, we assume that only a single noise source is present such as an equivalent white noise representing the large-signal noise factor of the RFA or an equivalent colored noise representing the PN injected by the RFA (and possibly other blocks) into the OEO loop. This noise is considered at the RHS of equation (3) as an additive term $a\varepsilon(t)$, where a is the RFA's voltage gain, and $\varepsilon(t)$ is the noise source injected at the RFA's input. Inserting this noise and the perturbed variable into equation (3) gives:

$$\begin{aligned}&z(t)*\left\{v\left(t+\alpha(t)\right)+\Delta v(t)\right\}=g\left(v\left(t-t_0+\alpha(t-t_0)\right)\right)\\&+h\left(v\left(t-t_0+\alpha(t-t_0)\right)\right)\Delta v(t-t_0)+a\varepsilon(t)\end{aligned} \quad (6)$$

where $h(v)=dg(v)/dv$.

2.3. System of equations in the spectrum domain

For small offset frequencies, the variation of the transfer function of the RF filter about the oscillation frequency is slow such that the following approximation holds [20-22]:

$$Z(k\omega_0+\Omega)\cong Z(k\omega_0)+\left.\frac{dZ}{d\omega}\right|_{k\omega_0}\Omega,\quad k=\pm1 \quad (7)$$

where Ω denotes the offset frequency from the carrier. This equation will be exploited shortly.

The spectrum vector (SV) of any variable is defined as a column vector containing the complex-valued Fourier series components of that variable [14-16]. The SV of a periodic variable is a constant vector, while that of a non-periodic one is a slowly-varying time-dependent vector. Because here only the fundamental harmonic is needed, as an example, the SV of $\Delta v(t)$ is equal to $\left[\Delta v_{-1}(t)\quad \Delta v_{+1}(t)\right]^T$ where T denotes the transpose, and $\Delta v_k(t)$ denotes the k'th Fourier series component of $\Delta v(t)$ whose maximum theoretical bandwidth is $\omega_0/2$.

By considering equations (6) and (7), examining the Fourier series components of the output of the blocks, and replacing the variables with their SVs, one arrives at the following SV domain equation (one can see, for example, the lemmas presented in [14] for a more detailed description):

$$\begin{aligned}&\mathbf{D}_{\alpha}(t)\left[\mathbf{T}_{\mathbf{Z}}^{\mathbf{0}}\mathbf{v}+\mathbf{T}_{\dot{\mathbf{Z}}}\mathbf{u_1}\frac{d\alpha}{dt}\right]+\mathbf{T}_{\mathbf{Z}}^{\mathbf{0}}\boldsymbol{\Delta}\mathbf{v}+\mathbf{T}_{\dot{\mathbf{Z}}}\frac{d\boldsymbol{\Delta}\mathbf{v}}{dt}=\\&\mathbf{D}_{\mathbf{t_0}}^{-\mathbf{1}}\mathbf{D}_{\alpha}(t-t_0)\left[\mathbf{g}+\mathbf{T}_{\mathbf{h}}\mathbf{D}_{\alpha}^{-\mathbf{1}}(t-t_0)\boldsymbol{\Delta}\mathbf{v}(t-t_0)\right]+a\boldsymbol{\varepsilon}(t)\end{aligned} \quad (8)$$

where $\mathbf{v}$, $\mathbf{g}$, $\boldsymbol{\varepsilon}(t)$, and $\boldsymbol{\Delta}\mathbf{v}$ are the SVs of $v(t)$, $g\left(v(t)\right)$, $\varepsilon(t)$, and $\Delta v(t)$ respectively, the column vector $\mathbf{u_1}$ is equal to

$j\omega_0 A\left[-1 \quad 1\right]^T/2$ (i.e., it is the SV of the time-derivative of $v(t)=A\cos(\omega_0 t)$), and the 2×2 matrices in equation (8) are defined by:

$$\left[\mathbf{T}_{\mathbf{Z}}^{\mathbf{0}}\right]_{n+H+1,l+H+1}=Z(n\omega_0)\delta_{n,l},\ n=\pm 1, l=\pm 1 \qquad (9)$$

$$\left[\mathbf{T}_{\mathbf{h}}\right]_{n+H+1,l+H+1}=h_{n-l},\ n=\pm 1, l=\pm 1 \qquad (10)$$

where h_k denotes the k'th Fourier series component of $h\left(v(t)\right)$, $Z(\omega)$ has been defined in equation (4), $\delta_{n,l}$ denotes the Kronecker delta, and H is the number of the harmonics considered in the analysis, which is here equal to 1. The diagonal matrices $\mathbf{D}_{\boldsymbol{\alpha}}(t)$, $\mathbf{D}_{t_0}$, and $\mathbf{T}_{\dot{\mathbf{Z}}}$ have similar structures as $\mathbf{T}_{\mathbf{Z}}^{\mathbf{0}}$ in equation (9), however, $Z(\omega)$ in equation (9) is replaced by $\exp\left(j\omega\alpha(t)\right)$, $\exp(j\omega t_0)$, and $-j\left(dZ(\omega)/d\omega\right)$, respectively.

For further proceeding, we use the fact that the SV domain form of equation (3) is $\mathbf{T}_{\mathbf{Z}}^{\mathbf{0}}\mathbf{v}=\mathbf{D}_{\mathbf{t_0}}^{-1}\mathbf{g}$. Using this equation in equation (8), multiplying both sides of the resulting equation by $\mathbf{D}_{\boldsymbol{\alpha}}^{-1}(t)$ from the left, and defining $\boldsymbol{\Delta}\mathbf{w}(t)=\mathbf{D}_{\boldsymbol{\alpha}}^{-1}(t)\boldsymbol{\Delta}\mathbf{v}(t)$, one arrives at:

$$\begin{aligned}&\mathbf{T}_{\dot{\mathbf{Z}}}\left[\mathbf{u}_1\frac{d\alpha}{dt}+\frac{d\boldsymbol{\Delta}\mathbf{w}}{dt}\right]+\mathbf{D}_{\mathbf{t_0}}^{-1}\left[\mathbf{I}-\mathbf{D}_{\boldsymbol{\alpha}}^{-1}(t)\mathbf{D}_{\boldsymbol{\alpha}}(t-t_0)\right]\mathbf{g}\\&+\mathbf{T}_{\mathbf{Z}_0}\boldsymbol{\Delta}\mathbf{w}-\mathbf{D}_{\mathbf{t_0}}^{-1}\mathbf{D}_{\boldsymbol{\alpha}}^{-1}(t)\mathbf{D}_{\boldsymbol{\alpha}}(t-t_0)\mathbf{T}_{\mathbf{h}}\boldsymbol{\Delta}\mathbf{w}(t-t_0)=\\&a\mathbf{D}_{\boldsymbol{\alpha}}^{-1}(t)\boldsymbol{\varepsilon}(t)\end{aligned} \qquad (11)$$

Note that in deriving equation (11), also the fact that $d\alpha/dt$ is a small-signal process (despite the large-signal nature of $\alpha(t)$) is used [18, 19]. Therefore we have approximated $\mathbf{D}_{\boldsymbol{\alpha}}^{-1}(t)\left(d\boldsymbol{\Delta}\mathbf{V}/dt\right)$ with $d\left(\mathbf{D}_{\boldsymbol{\alpha}}^{-1}(t)\boldsymbol{\Delta}\mathbf{V}\right)/dt$.

2.4. Extracting the PN SDDE

Now the SDDE governing the PN is extracted using the decomposition of the perturbation equations into the phase and orbital deviations as presented in [20-22] for conventional non-delay-based oscillators which is here called the HBPT. Taking the time-derivative of equation (3) and extracting the SVs of both sides gives:

$$\mathbf{J_0}\mathbf{u_1}=0,\quad \mathbf{J_0}=\mathbf{T}_{\mathbf{Z}}^{\mathbf{0}}-\mathbf{D}_{\mathbf{t_0}}^{-1}\mathbf{T}_{\mathbf{h}} \qquad (12)$$

where $\mathbf{u_1}$ has been defined after equation (8) and $\mathbf{J_0}$ is the so-called static Jacobian of the system [20-22]. Form equation (12), it is evident that $\mathbf{J_0}$ is singular and $\mathbf{u_1}$ is its right-hand null vector. Its left-hand null vector (here denoted by $\mathbf{v_1}$) is the SV version of the so-called Floquet eigenvector (defined in [18, 19]) in the frequency domain [20-22]. Therefore, we have $\mathbf{v_1^T J_0 = 0}$ which gives:

$$\mathbf{v}_1^{\mathbf{T}}\mathbf{T}_{\mathbf{Z}}^{\mathbf{0}}=\mathbf{v}_1^{\mathbf{T}}\mathbf{D}_{\mathbf{t_0}}^{-1}\mathbf{T}_{\mathbf{h}} \qquad (13)$$

Multiplying (11) by $\mathbf{v}_1^{\mathbf{T}}$ from the left and using equation (13), equation (14) is derived subject to the constraint given in equation (15).

$$\begin{aligned}&\mathbf{v}_1^{\mathbf{T}}\mathbf{T}_{\dot{\mathbf{Z}}}\mathbf{u}_1\frac{d\alpha}{dt}+\mathbf{v}_1^{\mathbf{T}}\mathbf{D}_{\mathbf{t_0}}^{-1}\left[\mathbf{I}-\mathbf{D}_{\boldsymbol{\alpha}}^{-1}(t)\mathbf{D}_{\boldsymbol{\alpha}}(t-t_0)\right]\mathbf{g}\\&=a\mathbf{v}_1^{\mathbf{T}}\mathbf{D}_{\boldsymbol{\alpha}}^{-1}(t)\boldsymbol{\varepsilon}(t)\end{aligned} \qquad (14)$$

$$\begin{aligned}&\mathbf{v}_1^{\mathbf{T}}\mathbf{T}_{\dot{\mathbf{Z}}}\frac{d\boldsymbol{\Delta}\mathbf{w}}{dt}+\\&\mathbf{v}_1^{\mathbf{T}}\mathbf{T}_{\mathbf{Z}_0}\left[\boldsymbol{\Delta}\mathbf{w}(t)-\mathbf{D}_{\boldsymbol{\alpha}}^{-1}(t)\mathbf{D}_{\boldsymbol{\alpha}}(t-t_0)\boldsymbol{\Delta}\mathbf{w}(t-t_0)\right]=0\end{aligned} \qquad (15)$$

Note that the system of equation (11) has three unknown variables ($\alpha(t)$ and the two components of $\Delta v(t)$) but with only

two scalar equations. Therefore, an extra constraint can be considered to find the solution as used in [20-22], which here is equation (15). This constraint changes the exact distribution of the power between the common PN and the orbital deviation process; however, it does not change the total noise power [20-22]. It is interesting to note that for the no-delay case (conventional electronic oscillators), the second term on the left hand side of equation (15) vanishes, and the constraint becomes similar to that presented in [20-22].

For further proceeding with equation (14), we extract the expressions for the matrix $\mathbf{T}_{\hat{\mathbf{Z}}}$ and the vector $\mathbf{v_1}$ as follows. The most commonly used transfer function (TF) for the RF-BPF is the model of the 2nd order filter with unity pass band response whose inverse TF is given by $Z(\omega)=1+jQ(\omega/\omega_r-\omega_r/\omega)$ [2, 3, 14] where Q and ω_r are the quality factor and the resonance frequency of the RF-BPF respectively. Usually, it is assumed in the analysis that the oscillation frequency is approximately equal to the resonance frequency of the filter i.e., $\omega_0=\omega_r$ [2, 3, 14-16]. By using this TF and the structure of $\mathbf{T}_{\hat{\mathbf{Z}}}$ defined after equation (10) it is easily seen that this matrix is equal to $2\mathbf{I}/B$, where $\mathbf{I}$ is the identity matrix and $B=\omega_r/Q$ is the angular bandwidth of the RF filter. Also, numerical analysis of the Jacobian matrix of (12) shows that $\mathbf{v_1}$ is a complex multiple of the vector $[1,-1]^T$. Here we can consider it equal to $[j,-j]^T$ for simplicity in deriving equations. Using the abovementioned structures for $\mathbf{T}_{\hat{\mathbf{Z}}}$ and $\mathbf{v_1}$ in equation (14), performing vector in matrix multiplications, using the fact that the components of $\mathbf{g}$ are $g_{\pm1}=A/2$, (14) is written as (see the appendix):

$$\frac{d\varphi}{dt}=-\frac{B}{2}\sin\left(\varphi(t)-\varphi(t-t_0)\right)+ j\frac{Ba}{2A}\left(e^{j\varphi(t)}\varepsilon_{-1}(t)-e^{-j\varphi(t)}\varepsilon_1(t)\right) \quad (16)$$

where $\varphi(t)=\omega_0\alpha(t)$ is the common PN process of the OEO, and the terms $\varepsilon_{\pm1}(t)$ are the Fourier series components of $\varepsilon(t)$ (also called its sidebands). Equation (16) is a form of the SDDE governing the PN. This equation is similar to equation (18) of [3]; however, with two minor differences: the sin term is replaced by its argument in [3], and the two sidebands of the noise source are not present in that reference.

Remark 1: A small-signal solution of equation (16) can be derived for a wide sense stationary noise by replacing the terms $\exp\left(\pm j\varphi(t)\right)$ with unity (through neglecting 2nd order differentials), replacing the sin function with its argument, finding the Fourier transform of $\varphi(t)$ through taking this transform of equation (16), computing the squared magnitude of this transform, and applying the stochastic mean operator. This gives the PN induced PSD versus the frequency offset f as:

$$\overline{|\hat{\varphi}|^2(f)}=\frac{1}{2}\left|\frac{Ba}{A\left(j2\pi f+\frac{B}{2}\left(1-e^{-j2\pi f t_0}\right)\right)}\right|^2\overline{|\hat{\varepsilon}|^2(f)} \quad (17)$$

where $\overline{|\hat{\varepsilon}|^2(f)}$ denotes the PSD of $\varepsilon(t)$. The predicted PN-PSD in equation (17) is exactly the same as equation (19) of [3] for additive noise sources. Note that the assumption that $\overline{|\hat{\varepsilon}_1|^2(f)}=\overline{|\hat{\varepsilon}_{-1}|^2(f)}=\overline{|\hat{\varepsilon}|^2(f)}$ is also used in deriving equation (17).

Remark 2: Up to now, the extracted formulations do not depend on the PSD shape of $\varepsilon(t)$, meaning that they are valid for both white and colored assumptions of $\varepsilon(t)$. Note that many noise sources act in an OEO. They include the white and flicker noise sources of the RFA and the PD [1-3] and the length-dependent noises of the optical part, such as the laser frequency noise and the high-frequency and low-frequency relative intensity noise (RIN) of the laser. The RIN may also be produced and augmented at the end of the fiber [4, 6]. Among these noise sources, the shot noises of the PD and RFA and the high-frequency RIN can be treated as white noise sources. Other noises such the PNs induced by the PD and the RFA can be considered as colored noise sources.

By transforming equation (16) into a standard SDDE, one can use the formulas presented in previous works specifically [18, 19] to resolve the oscillation spectrum. These works have used the stochastic calculus to resolve the PN-induced PSD of the output variable. We assume that the last term on the RHS of equation (16) is the low-frequency component of the product of a

semi-periodic function $y(t)$ with $\varepsilon(t)$. Thus its Fourier series components y_1 and y_{-1} are equal to the corresponding coefficients of $\exp\left(-j\varphi(t)\right)$ and $\exp\left(+j\varphi(t)\right)$ in equation (16), respectively. This observation gives $y(t) = -Ba\sin\left(\omega_0 t + \varphi(t)\right)/A$ hence equation (16) turns to:

$$\frac{d\varphi}{dt} = -\frac{B}{2}\sin\left(\varphi(t) - \varphi(t-t_0)\right) - \frac{Ba}{A}\sin\left(\omega_0 t + \varphi(t)\right)\varepsilon(t) \quad (18)$$

Note that the last term on the RHS of equation (18) also produces components at the harmonic frequency $2\omega_0$; however, because of the filtering nature of the dynamics of equation (18) (induced by the narrowband RF filter), it is practically filtered out.

Before solving equation (18) we assume that under the influence of practically small values of noise powers, the quantity $\varphi(t) - \varphi(t-t_0)$ is also very small therefore we may approximate equation (18) by:

$$\frac{d\varphi}{dt} = -\frac{B}{2}\left(\varphi(t) - \varphi(t-t_0)\right) - \frac{Ba}{A}\sin\left(\omega_0 t + \varphi(t)\right)\varepsilon(t) \quad (19)$$

3. COMPUTING THE OUTPUT PSD BASED ON THE SMALL-DELAY APPROXIMATION

Small delay approximation is a well-known method for solving SDDEs for cases where the time delay is small compared to the rate of the variations in a system [23, 24]. Since in delay-based OEOs, the product of the delay and the maximum offset frequency of interest may be several radians, in general, this delay cannot be considered small. However, for close-in offset frequencies where $\Omega t_0 << 1\ rad$, this approximation may give good results, as verified in the results section. This approximation is applied by replacing $\varphi(t-t_0)$ with its first-order Taylor approximation $\varphi(t) - (d\varphi/dt)t_0$. Therefore, equation (19) turns to:

$$\frac{d\alpha}{dt} = -a_0\sin\left(\omega_0\left(t + \alpha(t)\right)\right)\varepsilon(t), \quad a_0 = \frac{Ba}{A\omega_0\left(1 + Bt_0/2\right)} \quad (20)$$

where $\alpha(t)$ denotes the common time delay process. For solving the output PSD we separately consider two cases of having a white or a colored noise source as follows.

3.1. Exact output PSD in presence of a white noise source

First we consider the case where $\varepsilon(t)$ is a white Gaussian noise which may for example represent the effect of the large signal noise figure of the combination of the PD and the RFA. Then equation (20) can be written as:

$$\frac{d\alpha}{dt} = -a_0 k_n \sin\left(\omega_0\left(t + \alpha(t)\right)\right)\zeta(t) \quad (21)$$

Where $\zeta(t)$ is a standard unity-PSD white Gaussian noise process and k_n^2 denotes the constant PSD of $\varepsilon(t)$. Equation (20) is a special case of the main equation fully treated in [18, 19]; therefore, we can use the results of these references. Specifically equation (21) is a special case of equation (12) of [18]. It is proved in [18] that any variable of the free-running oscillator becomes stationary, asymptotically with time and the resulting stationary PSD of the output variable is given by equation (35) of this reference which is presented here for convenience as:

$$S(f)=\sum_{k=-\infty}^{\infty} X_k X_k^* \frac{f_0^2 k^2 c_w}{\pi^2 f_0^4 k^4 c_w^2+\left(f+kf_0\right)^2} \quad (22)$$

where f_0 is the oscillation frequency in Hertz, X_k is the k'th Fourier series component of the steady state signal (here $X_{\pm 1}=A/2$), and c_w is the time-average of the squared coefficient of $\zeta(t)$ at the RHS of equation (21), [18], which is:

$$c_w=\frac{1}{T}\int_0^T a_0^2 k_n^2 \sin^2(\omega_0\tau)d\tau=\frac{\left(a_0 k_n\right)^2}{2} \quad (23)$$

Where $T=2\pi/\omega_0$ is the oscillation period. The single-sided noise-to-carrier ratio (SSNCR) around an oscillation harmonic kf_0, at an offset frequency f_{off} is computed by substituting $f=kf_0+f_{off}$ in equation (22), and dividing the result with the carrier power $2|X_k|^2$. Especially for the fundamental harmonic, the SSNCR becomes [18, 19]:

$$L\left[f_{off}\right]=\frac{1}{2}\frac{f_0^2 c_w}{\pi^2 f_0^4 c_w^2+f_{off}^2} \quad (24)$$

As observed in equation (24), the output PSD has a Lorentzian shape and no longer goes to infinity at close-in offsets.

Remark 3: As an interesting observation, using the definition of c_w in equations (20) and (23), it is seen that the prediction of equation (24) for not very-close in offsets (where the constant value at the denominator can be neglected) is exactly half of the value given in equation (17) for small offsets where $\exp(-j2\pi t_0)\simeq 1-j2\pi t_0$. The half value is because equation (17) gives the PN PSD which is twice the SSNCR [18, 19].

Remark 4: As an important comparison, it should be noted that the Lorentzian shape is consistent with the predictions of [1] and [17]. The full width at half maximum (FWHM) of the PSD in equation (26a) of [1] is given as $\delta/\left(2\pi t_0^2\right)$, where δ is the ratio of the noise source PSD to the signal power. Now we show that the FWHM of the new approach is the same as that given in [1]. Using the definition of a_0 in equation (20) and taking the limit for $Bt_0>>1$ gives $a_0\simeq a/\left(\pi A f_0 t_0\right)$ and consequently $c_w\simeq k_n^2 a^2/\left(2(\pi A f_0 t_0)^2\right)$. The FWHM of $L\left[f_{off}\right]$ in equation (24) is $2\pi f_0^2 c_w$ Hz. Therefore, the FWHM of the new approach is given by

$$FWHM=\frac{1}{2\pi t_0^2}\frac{a^2 k_n^2}{\left(A^2/2\right)} \quad (25)$$

Note that the equivalent noise PSD at the output of the RFA is $\left(ak_n\right)^2$; therefore, one can easily identify the second fraction in equation (25) as δ. Consequently, equation (25) predicts the same FWHM as equation (26a) of [1], albeit for the case of $Bt_0>>1$. Regarding the PSD at close-in offsets, equation (29a) of [1] gives it as $S_{RF}(0)=4t_0^2/\delta$ and from our approach it is equal to $1/\left(2\pi^2 f_0^2 c_w\right)$ which simplifies to $2t_0^2/\delta$ of SSNCR or $4t_0^2/\delta$ of PN PSD for the case of $Bt_0>>1$. This is totally consistent with the results of [1]. However, only white noise sources have been treated in [1].

Reference [14] also predicts the same FWHM as in [1], however as inferred from equations (49) and (50) of [17], the PSD of the noise at close-in offsets is predicted as $S_{RF}(0)=\pi B^2 t_0^2/\delta$ which is different from both the new approach and that of [1]. Although [17] considers both white and colored noises, however, it only gives the non-singular PSD in the presence of the white noise sources. Here this non-singular PSD in the presence of both white and colored noises is computed using a completely different approach than those of [1, 17].

3.2. Asymptotic output PSD at small offset frequencies in presence of colored noises

Now we consider an example of a colored noise source which is the PN induced by the components of the microwave-photonic link such as the PD and the RFA. The open-loop injected PN $\varphi_{OL}(t)$ of these components results in the change of the state variable at RFA's output as $A\cos\left(\omega_0 t+\varphi(t)+\varphi_{OL}(t)\right)$. Using the small-signal nature of $\varphi_{OL}(t)$, an equivalent additive

noise is produced as $\varepsilon(t) = -A\sin\left(\omega_0\left(t+\alpha(t)\right)\right)\varphi_{OL}(t)$. Considering this noise and the previous white noise, changes equation (20) into:

$$\frac{d\alpha}{dt} = b_0 \sin^2\left(\omega_0\left(t+\alpha(t)\right)\right)\varphi_{OL}(t) - a_0 k_n \sin\left(\omega_0\left(t+\alpha(t)\right)\right)\zeta(t), \quad (26)$$

Where we have $b_0 = a_0 A / a$. A more general form of this equation has been treated in equation (64) of [19] where the coefficient of $\varphi_{OL}(t)$ and $\zeta(t)$ at the RHS of equation (26) can be any periodic function of $t+\alpha(t)$. The resulting spectrum has no analytical shape because of the complications of dealing with colored noise sources. However, its asymptotic behavior is given by equations (68) and (69) of [19] which result in the following SSNCR.

$$L\left[f_{off}\right] = \begin{cases} \frac{1}{2}\dfrac{f_0^2\left(c_w + |V_0|^2 S_{OL}(0)\right)}{\pi^2 f_0^4\left(c_w + |V_0|^2 S_{OL}(0)\right)^2 + f_{off}^2}, & f_{off} \approx 0 \\ \frac{1}{2}\dfrac{f_0^2}{f_{off}^2}\left(c_w + |V_0|^2 S_{OL}(f)\right), & f_{off} >> 0 \end{cases} \quad (27)$$

Where $S_{OL}(f)$ denotes the PSD of $\varphi_{OL}(t)$ and V_0 is the time-average of the coefficient of $\varphi_{OL}(t)$ at the RHS of equation (26) which is here equal to $V_0 = b_0/2$. Also c_w has been defined in equation (23). It should be noted that the expression of $L\left[f_{off}\right]$ at $f_{off} >> 0$ may not give accurate results for OEOs since at large offsets the small delay approximation is no longer valid. However, the expression at $f_{off} \approx 0$ is useful for having the correct non-singular value of the noise PSD at the close-in offsets.

In conclusion, accurate non-singular values of the PN-PSD at the close-in offset frequencies are given by equations (24) and (27) in the presence of just a white and white plus colored noises respectively.

4. RESULTS AND DISCUSSION

In this section, the validity of the presented analysis approach is further verified by comparing its predictions with the direct MCS in subsection A and the simulation results of [2] in subsection B.

4.1. Comparing results with MCS

In this subsection, the validity of the presented analysis approach is verified by comparing its results with the extensive MCS.

First we compare the results with the MCS for the case of having a white noise source as in equation (20).

The runtime of the MCS is proportional to $\omega_0/\Omega_{\min}$ where $\Omega_{\min}$ is the minimum frequency offset of interest. To avoid very large runtimes of the MCS, a hypothetical SLOEO with reduced frequency constants have been considered. The numerical parameters of the OEO in equation (2) are $v_\pi = 4$ V, $\phi_0 = 135^0$, $k_g = 3.06$ corresponding to a small-signal loop gain $-k_g \pi \cos(\phi_0)/v_\pi$ [14] equal to 1.7, the center frequency and bandwidth of the filter equal to $f_r = 25$ MHz and $B = 500$ KHz, respectively, and the fiber delay equal to $t_0 = 4.84\,\mu$S (corresponding to a free spectral range of 206.6 KHz).

The MCS is performed by using the Euler-Maruyama numerical scheme [25, 26] to find the solution of equation (20) where the increments of the stochastic delay are given by:

$$d\alpha = -a_0 \sin\left(\omega_0\left(t+\alpha(t)\right)\right)dw(t), \quad (28)$$

Where $dw(t)$ is the differential increment of the Wiener process which is a zero-mean Gaussian process with a standard

deviation equal to $\sqrt{dt}$. After finding the numerical values of $\alpha(t)$, the well-known Welch's algorithm [27] is used for computing the PSD of the variable $\exp\left(j\omega_0\alpha(t)\right)$. This PSD is the SSNCR. The time vector has been considered from zero to a final time t_f with the time-step dt. The following criteria have been considered for these quantities to avoid numerical inaccuracies.

$$dt < \min\left(\left\{\frac{1}{f_0}, \frac{1}{B}, \frac{1}{\max\left(f_{off}\right)}, t_0\right\}\right)/10 \qquad (29)$$

$$t_f > \max\left(\left\{\frac{1}{\min\left(f_{off}\right)}, 10t_0, \frac{10}{f_0}\right\}\right) \qquad (30)$$

Where $\max\left(f_{off}\right)$ and $\min\left(f_{off}\right)$ denote the maximum and the minimum frequency offsets considered in the analysis respectively.

The steady-state response of the OEO has been computed using the simple algorithm in [14] that gives $A = 2.5\,\mathrm{V}$ and considers $f_0 = f_r$.

Remark 5: when simulating the OEO, it is seen from the analytical PSD given by equation (24) that the FWHM is very small (in the order of a micro Hertz) for conventional noise values as reported in [1] and our simulations show (not presented here). Therefore, to see this flatness, one should simulate very small offset frequencies that makes the runtimes of the MCS prohibitively large. Hence the noise value $k_n = 8.9\times10^{-5}\ \mathrm{V}$ is used in this subsection which is about 10^5 times larger than the practical values at the RFA input so that this flatness occurs at larger offsets. This relaxes the runtime/memory requirements of the MCS.

Fig.2.

The computed PSD of the PN-induced output noise from the analytical formulation of [3] (equation (17)), the SDAA (equation (24)), and the MCS are presented in Fig.2.

It is seen that the results of the MCS have a very good matching with those of [3] at not close-in offsets. However, they have very good agreement with the results of the SDAA at close-in offsets, while the SDAA predicts inaccurate results at larger offsets. Therefore the SDAA can accurately compute the PN-induced PSD at close-in offsets.

Now we also compare the results of equation (27) with the MCS in case of having a colored noise as presented in equation (26). For better assessing the accuracy of this approach, the white noise $\zeta(t)$ in equation (26) is set to zero. For simplicity of the numerical simulations, we consider an Ornstein-Uhlenbeck process (OUP) as our colored noise source since it is easily simulated by a single SDE from the white noise. The PSD of the OUP is [28, 29]:

$$\overline{\tilde{\varphi}_{OL}^2(f)} = \frac{k_c^2}{1+\left(2\pi f / P_c\right)^2} \qquad (31)$$

Where it shows a low pass behavior. Considering the SDE that governs the OUP [28, 29], the following system of equations is numerically simulated to produce samples of $\alpha(t)$.

$$d\alpha = b_0 \sin^2\left(\omega_0\left(t+\alpha(t)\right)\right)\varphi_{OL}(t)\,dt \qquad (32)$$

$$d\varphi_{OL}(t) = -P_c\varphi_{OL}dt + P_c k_c dw(t) \qquad (33)$$

where $dw(t)$ is the differential of the Wiener process as explained after equation (28). Again the well-known Welch's algorithm [27] is used for computing the PSD of the variable $\exp\left(j\omega_0\alpha(t)\right)$ which gives the SSNCR.

For having reasonable runtimes and also being able to see the differences of the approaches, the following parameters have been considered. The oscillation frequency $f_0 = 1\mathrm{MHz}$, the RF filter's bandwidth $B = 2\pi\times500\,\mathrm{KHz}$ and the loop delay

$t_0 = 48.4\ \mu S$.

All the other parameters are as those of the previous OEO example. The pole of the noise PSD in (31) is set to $P_c = 2\pi \times 1\text{KHz}$.

The computed PSD of the PN-induced output noise from the first rule of equation (27) (denoted by the SDA), and the MCS are presented in Figures 3 and 4 for two different levels of $k_c\sqrt{p_c} = 0.1$ and $k_c\sqrt{p_c} = 10^{-6}$. Also the PN is simulated by the CMA of [30] where it can simulated the effect of the PN of the RFA on the output variable's PSD.

It is observed in Fig.3 that the results of the MCS have a very good agreement with those of the CMA at not close-in offsets. However, they have very good agreement with the results of the first rule of equation (27) (denoted by the SDA) at close-in offsets. In conclusion, without the first rule of equation (27), we are not able to compute the PSD at close-in offsets unless using the MCS. However, the MCS requires a prohibitively large runtime for practical GHz-range OEOs with very small noise powers.

Fig. 3.

It is observed in Fig. 4 that for these noise levels, the predictions of the first rule of equation (27) and the CMA converge with each other at small offset frequencies. Here the flatness of the PSD occurs at the very small offsets. However, simulating these offsets with the MCS becomes very time and memory-consuming therefore they have not been included in this figure. At larger offsets, the CMA results agree well with those of the MCS.

Remark 6: Based on the abovementioned results, for accurate estimation of the PN at all frequency offsets, one can simultaneously plot the PN PSD based on the first rule of equation (27) (called the SDAA) and half of the resulted values of equation (17). For small offset frequencies where equation (17) predicts larger values, the SDAA can be regarded as reliable and more accurate. However, for other offsets, equation (17) gives good results. Note that the SDAA can give accurate results from zero offsets to those located on the onset of the skirt of the first spurious peak caused by the delay. However, for larger offsets, only equation (17) is regarded as reliable. Also, the CMA approaches can be used for all offsets except the very close-in ones. Note that the reason for dividing the results of equation (17) with 2 (subtracting 3dB from it in decibel scale) is to get the PN PSD in dBc/Hz instead of dBrad^2/Hz [18, 19]"

4.2. Comparing results with another analysis approach in the literature

As another means for verifying the validity of the new approach, its results are compared with those presented in [2] for a SLOEO with a single white noise source. Here we just want to test the validity of the formulation and the hose-made computer code.

Fig.4.

The analysis approach of [2] is based on simulating many round trips of the envelope of the RF signal, taking the Fourier transform for computing the envelope's PSD at the end of each round trip, and finally averaging the resulting PSDs to compute the final PSD. Referring to equation (2), the numerical parameters of the OEO of [2] are $v_\pi = 3.14\ \text{V}$, $\phi_0 = 180^0$, and $k_g = 1.5$, corresponding to a small-signal loop gain $-k_g \pi \cos(\phi_0)/v_\pi$ [14] equal to 1.5, the center frequency and bandwidth of the filter equal to $f_r = 10\ \text{GHz}$ and $B/(2\pi) = 20\ \text{MHz}$, respectively, and the fiber delay equal to $t_0 = 0.28\mu\text{S}$. A white noise source with PSD equal to $\rho_N = 10^{-20}\ \text{W/Hz}$ is considered at the RFA input, and the voltage gain of the RFA is $a = 7.5$. In our simulations, a voltage noise source with PSD equal to $k_n^2 = \rho_N R$ is considered in the analysis, where $R = 50\,\Omega$ is the input impedance of the RFA. The presented PSD of the output variable from Figure 4 of [2] is compared with the simulated results from the new approach (equation (24)) in Fig. 5. It is seen that the results of equation (17) (denoted by Chembo) has a very good agreement with [2]. Also the results of the SDAA match these results at small offsets. This verifies the accuracy of our formulation and its computer implementation.

As a final comparison, the characteristics and features of the presented approach are compared with those of the previously published methods in Table 1. From this table, it is seen that the new approach and those of [1,17] are the only approaches that predict non-singular PSDs at close-in offsets. However, [1] is limited to white noises while the new approach takes both white and colored noises into account. Also, as mentioned after remark 4, [17] predicts the same FWHM in the presence of the white noises as the new approach but with a different asymptotic close-in PN than the new approach and [1]. Also, the close-in PN in the presence of the colored noises has not been presented in [17]. Finally based on remark 6 (located at the end of subsection 4.1) using both the new approach in conjunction with equation (17) (i.e. the method of [3]) can give a complete picture of the PN at

every offset frequency.

5. CONCLUSIONS

An analysis approach was proposed for simulating the PN-induced PSD of the output variables in the delay-based SLOEOs at the close-in frequency offsets. First, a systematic perturbation method was used to extract the SDDE governing the PN process in a single-loop delay-based OEO. Then this SDDE was approximated by an SODE using the small-delay approximation which is valid for small frequency offsets. This resulting PSD of the output variables was obtained based on the previously published formulations. This approach gives an analytical formulation that can accurately compute the output PSD at close-in offset frequencies but not at larger ones. This method overcomes the singularity problem of the output PSD at close-in offsets as opposed to the classical noise analysis approaches in OEOs that are based on the small-signal assumption of the PN. The validity of this approach was verified by comparing its results with full MCS, previously published formulations, and simulation results in the literature.

Table 1: Comparison of the new approach with the PN analysis approaches presented in the literature

Fig.5.

APPENDIX

We first simplify the terms in equation (14). Considering the mentioned structures at the paragraph following equation (15) we have:

$$\mathbf{v_1^T T_{\hat{2}} u_1} = \begin{bmatrix} j & -j \end{bmatrix} \begin{bmatrix} \frac{2}{B} & 0 \\ 0 & \frac{2}{B} \end{bmatrix} \begin{bmatrix} -j\omega_0 \frac{A}{2} \\ +j\omega_0 \frac{A}{2} \end{bmatrix} = 2\omega_0 \frac{A}{B} \tag{a1}$$

$$\mathbf{v_1^T D_{t_0}^{-1}} \left[\mathbf{I} - \mathbf{D_\alpha^{-1}}(t) \mathbf{D}_\alpha (t - t_0) \right] \mathbf{g} = \begin{bmatrix} j & -j \end{bmatrix} \times$$
$$\begin{bmatrix} 1 - \exp\left(-j\omega_0 \left(\alpha(t-t_0) - \alpha(t)\right)\right) & 0 \\ 0 & 1 - \exp\left(+j\omega_0 \left(\alpha(t-t_0) - \alpha(t)\right)\right) \end{bmatrix} \begin{bmatrix} A/2 \\ A/2 \end{bmatrix} \tag{a2}$$
$$= A \sin\left(\omega_0 \left(\alpha(t) - \alpha(t-t_0)\right)\right)$$

$$a \mathbf{v_1^T D_\alpha^{-1}}(t) \boldsymbol{\varepsilon}(t) =$$
$$a \begin{bmatrix} j & -j \end{bmatrix} \begin{bmatrix} \exp\left(+j\omega_0 \alpha(t)\right) & 0 \\ 0 & \exp\left(-j\omega_0 \alpha(t)\right) \end{bmatrix} \begin{bmatrix} \varepsilon_{-1}(t) \\ \varepsilon_{+1}(t) \end{bmatrix} = \tag{a3}$$
$$ja\varepsilon_{-1} \exp\left(-j\varphi\alpha(t)\right) - ja\varepsilon_1 \exp\left(j\varphi\alpha(t)\right)$$

Note that in deriving equation (a2) we have used the fact that the total phase shift of the OEO loop at the oscillation frequency $\omega_0 t_0$ is an integer multiple of 2π therefore we have $\mathbf{D_{t_0}} = \mathbf{I}$. Using (a1) to (a3) in (14) one arrive at:

$$2\omega_0 \frac{A}{B} \frac{d\alpha}{dt} + A \sin\left(\omega_0 \left(\alpha(t) - \alpha(t-t_0)\right)\right) =$$
$$ja\varepsilon_{-1}(t) \exp\left(+j\omega_0 \alpha(t)\right) - ja\varepsilon_1(t) \exp\left(-j\omega_0 \alpha(t)\right) \tag{a4}$$

Dividing both sides of (a4) with $2A/B$ and using $\varphi(t) = \omega_0 \alpha(t)$ results in equation (16).

REFERENCES

1. Yao, X. S. and Maleki, L. "Optoelectronic microwave oscillator", *J. Opt. Soc. Am. B*, **13**(8), pp. 1725-1735 (1996). (doi: 10.1364/JOSAB.13.001725)

2. Levy, E. C., Horowitz, M., and Menyuk, C. R. "Modeling optoelectronic oscillators", *J. Opt. Soc. Am. B*, **26**(1), pp. 148-159 (2009). (doi: 10.1364/JOSAB.26.000148).
3. Chembo, Y. K., Volyanskiy, K., Larger, L., et. al. "Determination of phase noise spectra in optoelectronic microwave oscillators: a Langevin approach", *IEEE J. Quantum Electron*., **45**(2), pp. 178-186 (2009). (doi: 10.1109/JQE.2008.2002666).
4. Lelièvre, O., Crozatier,V., Berger P., et. al. "A model for designing ultralow noise single-and dual-loop 10-GHz optoelectronic oscillators", *J. Light. Technol*., **35**(20), pp. 4366-4374 (2017). (doi: 10.1109/JLT.2017.2729018).
5. Wang X., and Yao, X. S. "Phase-locked opto-electronic oscillator (OEO) of ultralow phase noise with record-low Allan deviation of 3.4$\times $${10}^{-14} $ at 1 s.", *IEEE Trans. Microw. Theory. Tech* , **71**(12), pp. 5381 - 5392 (2023). (doi: 10.1109/TMTT.2023.3278934).
6. Mikitchuk, K., Chizh, A., and Malyshev, S. "Modeling and design of delay-line optoelectronic oscillators", *IEEE J. Quantum Electron*., **52**(10), pp. 1-8, (2016). (doi: 10.1109/JQE.2016.2600408).
7. Chembo, Y. K., Brunner D., Jacquot, M., et. al. "Optoelectronic oscillators with time-delayed feedback", *Rev. Mod. Phys.* **91**(3), pp. 035006 (2019). (doi: 10.1103/RevModPhys.91.035006).
8. Peng, H., Lei, P., Xie, X., et. al. "Photonic RF synthesizer based on a phase-locked optoelectronic oscillator using anti-Stokes loss spectrum of stimulated Brillouin scattering", *IEEE Photon. J*., **14**(3), pp. 1-8 (2022). (doi: 10.1109/JPHOT.2022.3174921).
9. Wang, Y., Shuang, O., Yang, M., et. al., "Wideband frequency-tunable optoelectronic oscillator with ultra-narrow linewidth based on stimulated Brillouin scattering", Opt. Commun., **546**, pp. 129734, 2023. (doi: 10.1016/j.optcom.2023.129734).
10. Li, M., Li, L., Cao R., et. al., "Optoelectronic oscillator with improved sidemode suppression by joint use of spectral Vernier effect and parity-time symmetry", *Opt. Express*, **30**(16), pp. 28774-28782 (2022). (doi: 10.1364/OE.460524).
11. Fu, J., Dai, Z., Han, X., et. al. "Wavelength-space parity-time symmetric optoelectronic oscillator using a chirped fiber Bragg grating", *IEEE Photon. Technol. Lett.* **36**(3), pp. 187-190, (2024). (Appeared online on 18 December 2023). (doi: 10.1109/LPT.2023.3344683).
12. Nguewou-Hyousse, H., and Chembo, Y. K. "Stochastic analysis of miniature optoelectronic oscillators based on whispering-gallery mode electrooptical modulators", *IEEE Photon. J.*, **13**(3), pp. 1-10, 2021. (doi: 10.1109/JPHOT.2021.3070846).
13. Ha, M., and Chembo, Y. K. "On the universality of microwave envelope equations for narrowband optoelectronic oscillators", *J. Light. Technol*., **40**(18), pp. 6131-6138, (2022). (doi: 10.1109/JLT.2022.3190695).
14. Jahanbakht, S. "Noise spectrum characterization of optoelectronic oscillators in the presence of laser frequency noise", *Appl. Opt*., **55**(8), pp. 1854-1862, (2016). (doi: 10.1364/AO.55.001854).
15. Jahanbakht, S. "Frequency-domain analysis of optoelectronic oscillators utilizing optical and RF resonators with arbitrary transfer functions", *J. Opt. Soc. Am. B*, **38**(10), pp. 2813-2822, (2021). (doi: 10.1364/JOSAB.435698).
16. Rahimi, M.M., and Jahanbakht, S. "Frequency-domain analysis of dual-loop optoelectronic oscillators", *Appl. Opt*., **60**(36), pp. 11125-11133, (2021). (doi: 10.1364/AO.444345).
17. Banerjee, A., Aguiar Dantas de Britto, A., L., and Mendes Pacheco G. "Computation of phase noise spectrum in optoelectronic oscillator" *IEEE J. Quantum Electron*., **57**(3), pp. 1-13 (2021). (doi: 10.1109/JQE.2021.3065530).
18. Demir,A., Mehrotra, A., and Roychowdhury, J. "Phase noise in oscillators: A unifying theory and numerical methods for characterization", *IEEE Trans. Circuits Syst. I Regul. Pap.*, **47**(5), pp. 655-674 (2000). (doi: 10.1109/81.847872).
19. Demir, A. "Phase noise and timing jitter in oscillators with colored-noise sources", *IEEE Trans. Circuits Syst. I Regul. Pap.*, **49**(12), pp. 1782-1791 (2002). (doi: 10.1109/TCSI.2002.805707).
20. Sancho, S., Suarez, A., and Ramirez, F. "Phase and amplitude noise analysis in microwave oscillators using nodal harmonic balance." *IEEE Trans. Microw. Theory. Tech*., **55**(7), pp. 1568-1583 (2007). (doi: 10.1109/TMTT.2007.900213).
21. Sancho, S., Suarez, A., Dominguez, J., et. al. "Analysis of near-carrier phase-noise spectrum in free-running oscillators in the presence of white and colored noise sources", *IEEE Trans. Microw. Theory. Tech*., **58**(3), pp. 587-601, (2010). (doi: 10.1109/TMTT.2010.2040326).
22. Jahanbakht, S., and Farzaneh, F. "Computation of the phase and amplitude noise in microwave oscillators and a simplified calculation method for far enough from the carrier offsets", *IET Microw. Antennas Propag*., **4**(12), pp. 2031-2041 (2010). (doi: 10.1049/iet-map.2009.0396).
23. Guillouzic, S., L'Heureux, I., and Longtin, A. "Small delay approximation of stochastic delay differential equations", *Phys. Rev. E*, **59**(4), pp. 3970 (1999). (doi: 10.1103/PhysRevE.59.3970).
24. A. Longtin, "Stochastic delay-differential equations." *In Complex Time-delay Systems*, pp. 177-195., Springer, Berlin, Germany, (2009). (doi: 10.1007/978-3-642-02329-3_6).
25. Kloeden, P. E., Platen, E., and Schurz, H., "Strong approximations" in *Numerical solution of SDE through computer experiments* , 1st Edn., pp. 139-178, Springer-Verlag, Berlin, Germany, (2012). (doi: 10.1007/978-3-642-57913-4)
26. Baker, C. T., and Buckwar, E. "Numerical analysis of explicit one-step methods for stochastic delay differential equations", *LMS J. Comput. Math*., **3**, pp. 315-335 (2000). (doi: 10.1112/S1461157000000322).
27. Oppenheim, A. V., and Schafer, R. W. "Power spectrum estimation" in *Digital signal processing*, 1st Edn,, pp. 532-577, Prentice-Hall, Englewood Cliffs, NJ, USA (1975).
28. C. W. Gardiner, "The Ito calculus and stochastic differential equations" in *Handbook of stochastic methods for physics, chemistry and the natural sciences*, 3rd Edn., pp. 80-115, Springer verlag, Berlin, Heidelberg, New York:, 2004,.

29. Abtahi, A. S., and Jahanbakht, S. "Frequency-domain behavioural noise analysis of analogue phase-locked loops", *IET Microw. Antennas Propag*. **14**(14), pp. 1909-1917 (2020). (doi: 10.1049/iet-map.2020.0672).
30. Jahanbakht, S., Hosseini, S. E., and Banai, A. "Prediction of the noise spectrum in optoelectronic oscillators: an analytical conversion matrix approach", *J. Opt. Soc. Am. B*, **31**(8), pp. 1915-1925 (2014). (doi: 10.1364/JOSAB.31.001915).

List of figure captions:

Fig. 1: The schematic of the delay-based single-loop optoelectronic oscillator [2,3,14]. Abbreviations are: CW: Continuous wave, and RF: Radio frequency.

Fig. 2. The computed output power spectral density from [3] (denoted by Chembo), the small delay approximation approach (SDAA), and the Monte Carlo simulation (MCS).

Fig. 3. The computed power spectral density of the phase noise-induced output noise from the small delay approximation approach (SDAA) (i.e. the first rule of equation (27)), the conversion matrix approach (CMA), and the Monte Carlo simulation (MCS) for $k_c\sqrt{p_c}=0.1$

Fig. 4. The computed power spectral density of the phase noise-induced output noise from the small delay approximation approach (SDAA) (i.e. the first rule of equation (27)), the conversion matrix approach (CMA), and the Monte Carlo simulation (MCS) for $k_c\sqrt{p_c}=10^{-6}$.

Fig. 5. Comparison of the output power spectral density of the single-loop optoelectronic oscillator case of [2] from this reference (denoted by Levy), from Eq. (17) (denoted by Chembo), and the small delay approximation approach (SDAA).

List of table captions:

Table 1: Comparison of the new approach with the phase noise analysis approaches presented in the literature. Abbreviations are: CMA: conversion matrix approach, PN: phase noise, SDDE: stochastic delay differential equation, SDAA: small delay approximation approach.

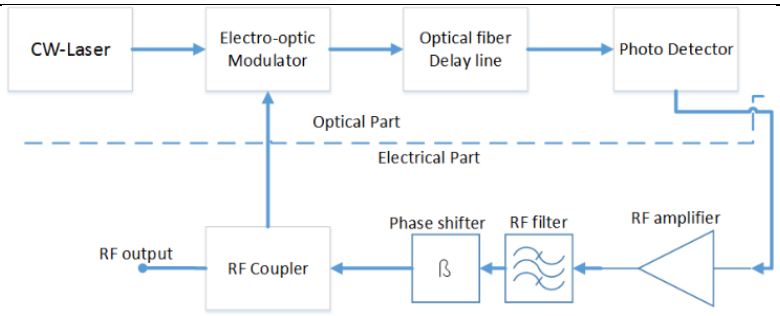

Figure 1

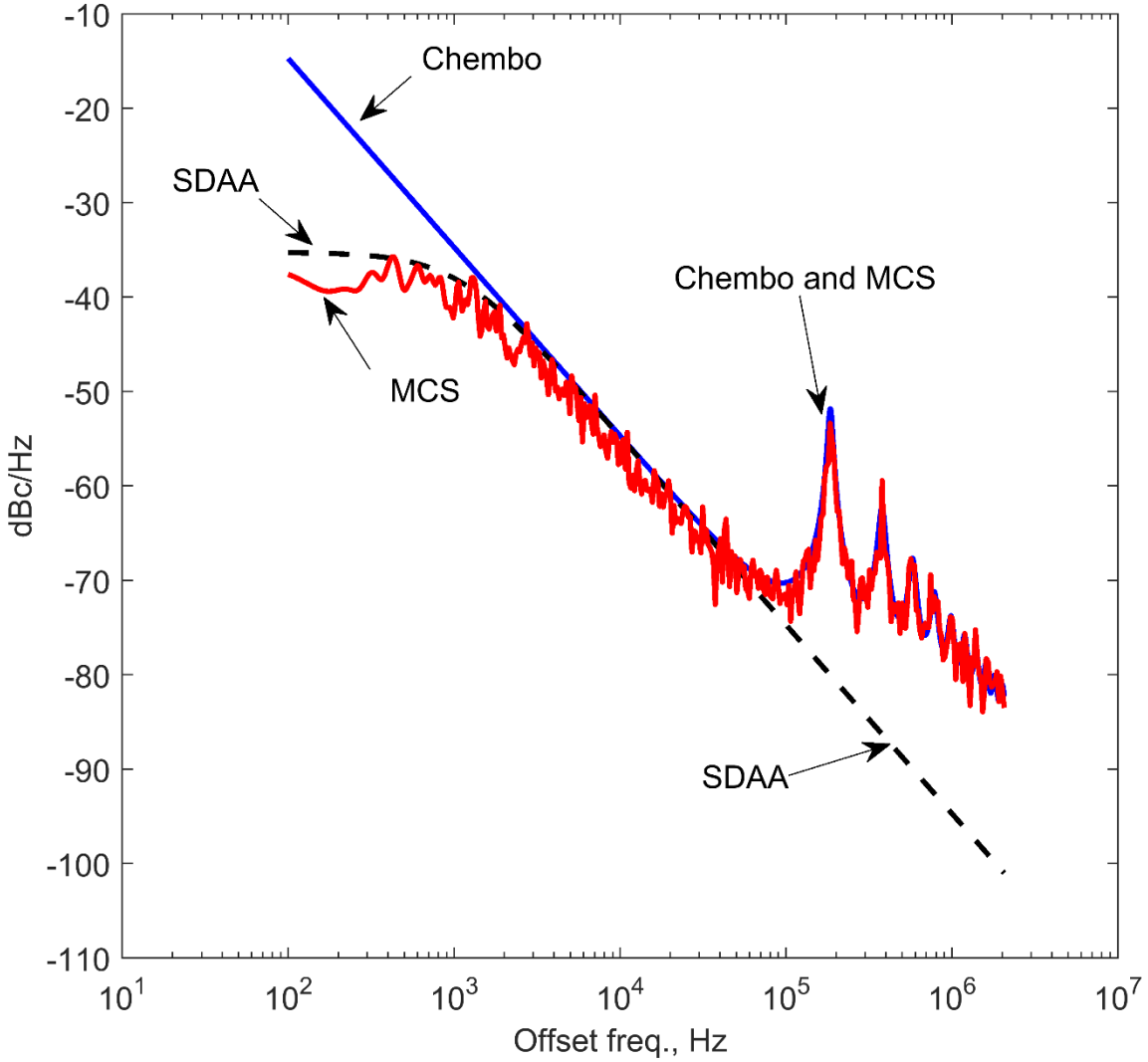
-10
-20
-30
-40
-50
-60
-70
-80
-90
-100
-110
dBc/Hz
10^1
10^2
10^3
10^4
10^5
10^6
10^7
Offset freq., Hz
Chembo
SDAA
MCS
Chembo and MCS
SDAA

Figure 2

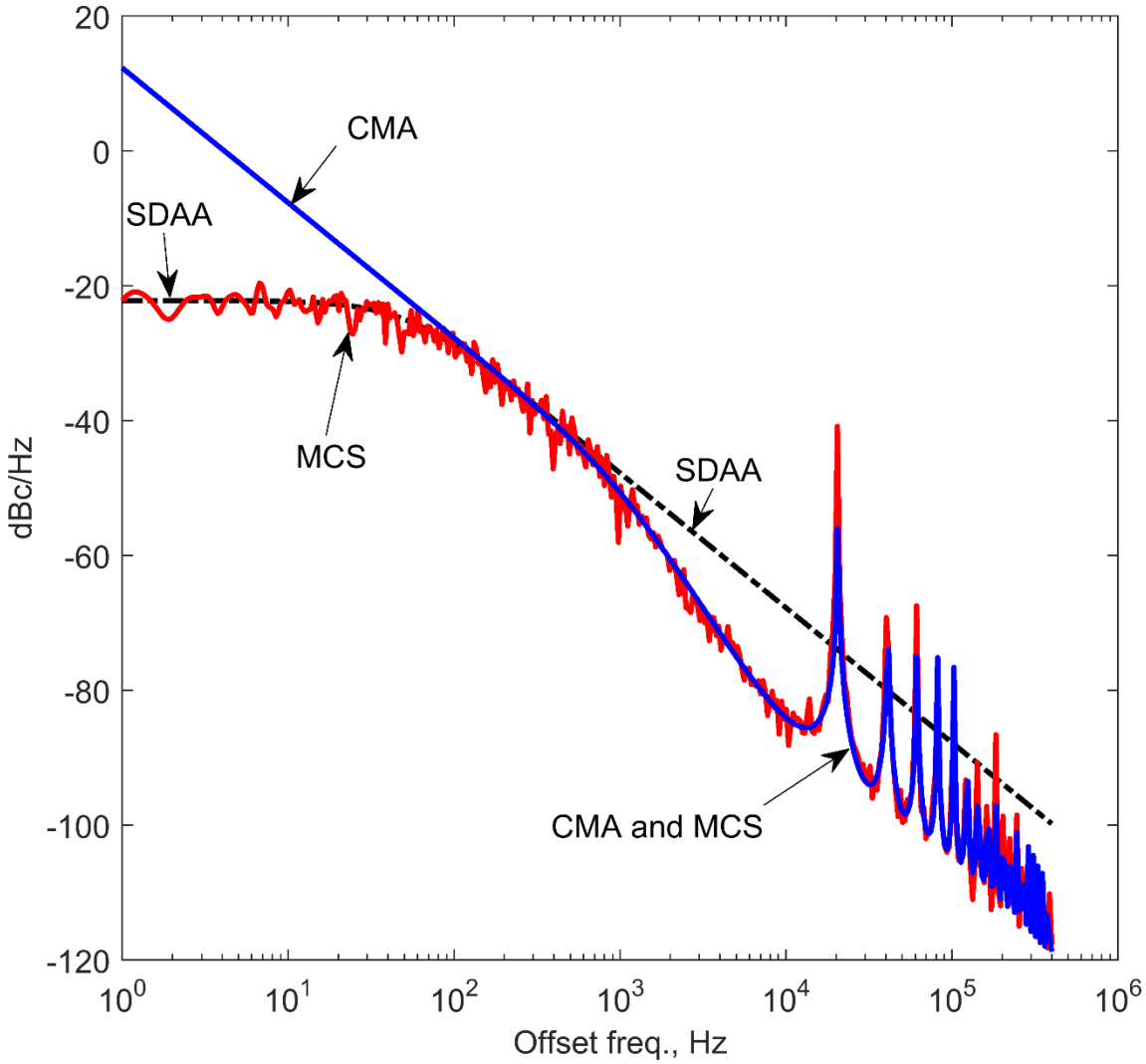
20
0
-20
-40
-60
-80
-100
-120
dBc/Hz
CMA
SDAA
MCS
SDAA
CMA and MCS
10^0
10^1
10^2
10^3
10^4
10^5
10^6
Offset freq., Hz

Figure 3

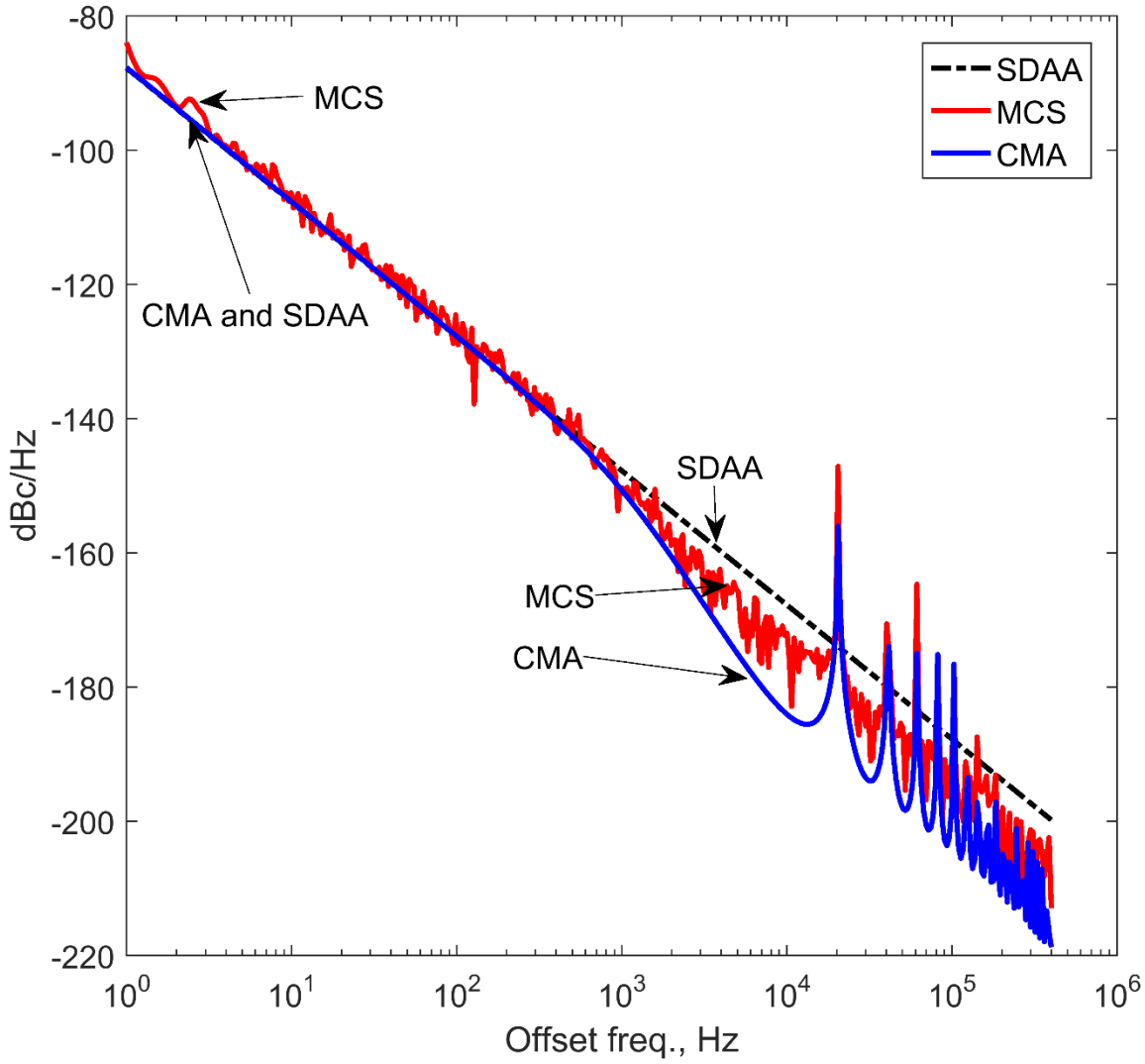
SDAA
MCS
CMA
MCS
CMA and SDAA
SDAA
MCS
CMA
dBc/Hz
Offset freq., Hz
-80
-100
-120
-140
-160
-180
-200
-220
10^0
10^1
10^2
10^3
10^4
10^5
10^6

Figure 4

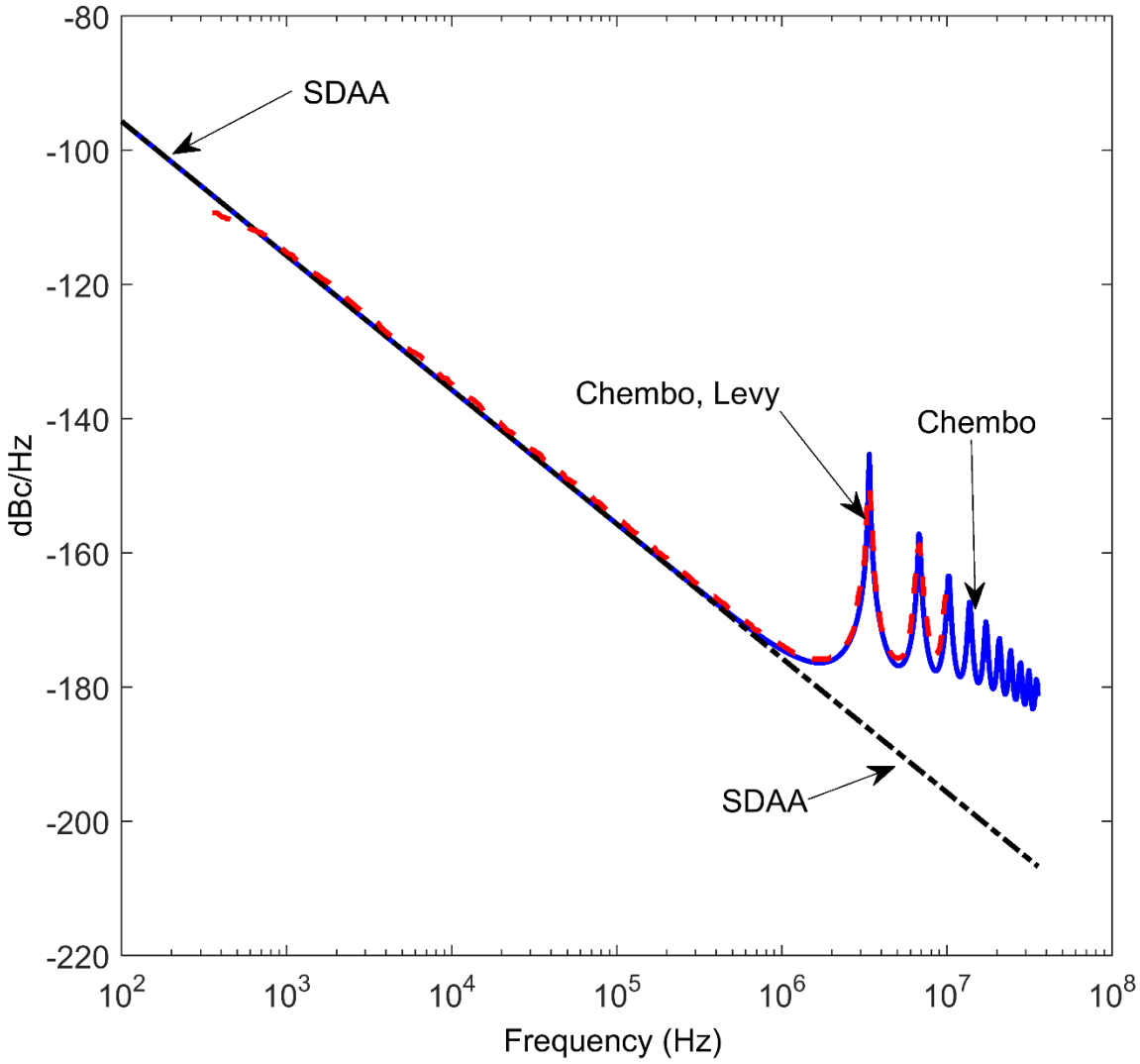
-80
-100
-120
-140
-160
-180
-200
-220
dBc/Hz
SDAA
Chembo, Levy
Chembo
SDAA
10^2
10^3
10^4
10^5
10^6
10^7
10^8
Frequency (Hz)

Figure 5

Table 1:

Method / Characteristics	SDAA (this paper)	[3, 13], (Eq. (17))	[1]	[17]	[4, 5]	[14-16]	[2, 6]
Approach	Small delay approximation to the PN-SDDE	analysis of the PN-SDDE with small-signal assumption of PN	Regenerative feedback approach	Injection locking/pulling approach	PN transfer model	CMA	Envelope domain transient analysis
White/colored noise	both	both	white	both	both	both	White. Special kinds of colored noises.
Singularity at close-in offsets	no	yes	no	no	yes	yes	yes
Offsets where the results are Accurate	From zero to the onset of the skirt of the first spurious peak	All but not very close-in ones	All offsets	All offsets	All but not very close-in ones	All but not very close-in ones	All but not very close-in ones
Runtime at a single frequency offset	<1mS	<1mS	<1mS	<1mS	<1mS	<1mS	In the order of 10 minutes for offsets larger than 1kHz

Biographies:

Sajad Jahanbakht is an associate Professor at the University of Kashan, Iran. He received his BS degree in electronic engineering from Isfahan University of Technology and MS, and PhD degrees in microwave and optical engineering from Sharif University of Technology. His main research interest is the simulation and optimization of the signal, stability, and noise performance of nonlinear active microwave and optoelectronic circuits. He is also interested in the simulation and design of passive microwave circuits and antennas.